Author Manuscript

Author Manuscript

Author Manuscript

Author Manuscript

HHS Public Access

Author manuscript

Exp Eye Res. Author manuscript; available in PMC 2023 June 01.

Published in final edited form as:

Exp Eye Res. 2022 June ; 219: 109030. doi:10.1016/j.exer.2022.109030.

Morphological Changes to Schlemm's Canal and the Distal Aqueous Outflow Pathway in Monkey Eyes with Laser-Induced Ocular Hypertension

Shayna Sosnowik[1], **David L. Swain**[1,2], **Shan Fan**[3], **Carol B. Toris**[3,4], **Haiyan Gong**[1,2]

[1]Department of Ophthalmology, Boston University School of Medicine, Boston, MA, USA

[2]Department of Anatomy and Neurobiology, Boston University School of Medicine, Boston, MA, USA

[3]Department of Ophthalmology and Visual Science, University of Nebraska Medical Center, Omaha, NE, USA

[4]Department of Ophthalmology and Visual Sciences, The Ohio State University, Columbus, OH, USA.

Abstract

Though roughly 30–50% of aqueous outflow resistance resides distal to Schlemm's canal (SC), the morphology of the conventional outflow pathway distal to SC has not been thoroughly evaluated. This study examined the morphological changes along proximal and distal aspects of the conventional aqueous outflow pathway and their association with decreased outflow facility in an experimental model of glaucoma in cynomolgus macaques. Nd:YAG laser burns were made to 270–340 degrees of the trabecular meshwork (TM) of one eye ($n = 6$) or both eyes ($n = 2$) of each monkey to induce ocular hypertension. Distinct regions of the TM were left unlasered. Contralateral eyes ($n = 5$) were not lasered and were utilized as controls. Monkeys were sacrificed ≥ 60 months after their last laser treatment. All eyes were enucleated and perfused at 15 mmHg for 30 minutes to measure outflow facility. Two pairs of eyes were also perfused with fluorescein to examine segmental outflow. All eyes underwent perfusion-fixation for 1 hr. Anterior segments were cut into radial wedges and processed for light and electron microscopy. Width, height, and cross-sectional area (CSA) of SC were compared between high- and low-flow regions of control eyes, and between non-lasered regions of laser-treated eyes and control eyes. Number and CSA of intrascleral veins (ISVs) were compared between non-lasered and lasered regions of laser-treated eyes and control eyes, and between high- and low-flow regions of control eyes. Scleral collagen fibril diameter was compared between control eyes and lasered and non-lasered regions of laser-treated eyes. Median outflow facility was significantly decreased in laser-treated eyes compared to

Correspondence: Haiyan Gong, MD, PhD, Department of Ophthalmology, Boston University School of Medicine, 72 East Concord St. Room L-905, Boston, MA 02118, USA, hgong@bu.edu.

Declaration of competing interest

The authors declare no conflicts of interest

Publisher's Disclaimer: This is a PDF file of an unedited manuscript that has been accepted for publication. As a service to our customers we are providing this early version of the manuscript. The manuscript will undergo copyediting, typesetting, and review of the resulting proof before it is published in its final form. Please note that during the production process errors may be discovered which could affect the content, and all legal disclaimers that apply to the journal pertain.

Author Manuscript Author Manuscript Author Manuscript Author Manuscript

control eyes ($P = 0.02$). Median CSA and height of SC were smaller in high- flow regions than low-flow regions of control eyes ($P < 0.05$). Median width of SC was not significantly different between high- and low-flow regions of control eyes ($P > 0.05$). Median CSA, width, and height of SC were not different between non-lasered regions and control eyes ($P > 0.05$). SC was partially or completely obliterated in lasered regions. Median number of ISVs was significantly decreased in lasered regions compared to non-lasered regions ($P < 0.01$) and control eyes ($P < 0.01$). Median CSA of ISVs did not differ between these groups ($P > 0.05$). Median number and CSA of ISVs were not significantly different between high- and low-flow regions of control eyes ($P > 0.05$). Lasered regions displayed looser scleral stroma and smaller median diameter of collagen fibrils adjacent to the TM compared to non-lasered regions ($P < 0.05$) and control eyes ($P < 0.05$). Dense TM, partial to complete obliteration of SC, and a decreased number of patent ISVs may account in part for the decreased outflow facility in monkey eyes with laser-induced ocular hypertension. The significance of changes in scleral structure in laser-treated eyes warrants further investigation.

Keywords

laser-induced ocular hypertension; trabecular meshwork; Schlemm's canal; intrascleral vein; intraocular pressure; aqueous outflow facility; segmental outflow; monkey eye

1. Introduction

Glaucoma is a degenerative optic neuropathy characterized by the loss of optic nerve axons and retinal ganglion cells. Primary open-angle glaucoma (POAG), a class of glaucoma in which the iridocorneal angle is unobstructed, is the second most common cause of blindness in the United States (Weinreb et al., 2016). The only modifiable risk factor for the development of POAG is elevation of intraocular pressure (IOP) due to increased outflow resistance (AGIS, 2000). Current medical and surgical therapy of POAG focuses on reduction of IOP. Therefore, understanding the sources of increased outflow resistance that contribute to IOP elevation in POAG is critical (Kwon et al., 2009). As the outflow facility in the trabecular outflow pathway is about 10 times that of the uveoscleral outflow pathway, sources of resistance in and downstream of the TM are of particular interest (Bill, 1966; Toris and Pederson, 1985).

Most outflow resistance in the conventional outflow pathway is thought to be localized to the juxtacanalicular connective tissue (JCT) and the inner wall of Schlemm's canal (SC) (Grant, 1963; Mäepea and Bill, 1992, 1989; Vahabikashi et al., 2019). At the level of the JCT, resistance may be modulated by a funneling effect of the pores in the inner wall of SC (Johnson et al., 1992). Other evidence suggests approximately 30% to 50% of outflow resistance actually may lie distal to SC (Grant, 1963; Rosenquist et al., 1989; Schuman et al., 1999). In normal human donor eyes, excimer laser ablation from the sclera through the outer wall of SC eliminated 35% of outflow resistance, suggesting that this resistance could be attributed to the outflow pathway distal to SC (Schuman et al., 1999). In addition, trabeculotomy in normal enucleated human eyes perfused at pressures between 15–25 mmHg decreased resistance by 77%, suggesting that approximately 23% of outflow resistance may lie distal to SC (Grant, 1963). In a study performing complete

Author Manuscript Author Manuscript Author Manuscript Author Manuscript

trabeculotomies on normal enucleated human eyes, a 49% decrease in resistance was found at a perfusion pressure of 7 mmHg. Interestingly, given that the episcleral venous pressure in enucleated human eyes is 0 mmHg, a perfusion pressure of 7 mmHg is more representative of a normal physiologic pressure difference across the inner wall of SC, and thus up to 51% of outflow resistance may lie distal to SC in normal human eyes (Rosenquist et al., 1989).

The role of the distal outflow pathway in generating outflow resistance in POAG eyes remains unclear. In one study, trabeculotomy in enucleated human POAG eyes normalized outflow facility, suggesting that the source of increased outflow resistance in POAG eyes lies overwhelmingly within the trabecular meshwork (TM) (Grant, 1963). However, procedures intended to bypass resistance in the TM, such as *ab interno* trabeculectomy and iStent placement, have not achieved the same degree of IOP reduction as conventional trabeculectomies (Arriola-Villalobos et al., 2012; Jea et al., 2012; Minckler et al., 2005; Swaminathan et al., 2014). Given the lack of consensus, further evaluation of possible sources of resistance in the distal outflow pathway in POAG eyes is warranted.

The purpose of this study was to evaluate the morphological changes along the conventional outflow pathway and how they may contribute to decreased outflow facility or increased outflow resistance in an experimental animal model of POAG. Currently, one of the best experimental animal models of POAG establishes ocular hypertension/glaucoma in monkeys via circumferential photocoagulation of the TM (Gaasterland and Kupfer, 1974; Pederson and Gaasterland, 1984; Radius and Pederson, 1984). This model is a useful tool to understand human POAG for several reasons. This model mimics aspects of POAG through a noninvasive procedure that produces only transient inflammation and alters a specific region of the outflow pathway (Gaasterland and Kupfer, 1974). Human and monkey eyes have similar anatomy and physiology of the iridocorneal angle. The model demonstrates progressive optic nerve cupping, ganglion cell and axonal loss, and decreased outflow facility. Additionally, the model responds to topical ocular hypotensive drugs in a manner similar to humans, making it useful for preclinical testing of new glaucoma therapies (Gaasterland and Kupfer, 1974; Lee et al., 1987; Pederson and Gaasterland, 1984; Radius and Pederson, 1984). For these reasons, the lasered monkey model of ocular hypertension was utilized in this study.

To identify regions of aqueous outflow resistance in the monkey model, we established a method for identifying regions of active drainage. Previous tracer studies of conventional outflow in the lasered monkey model found that cationised ferritin and fluorescent microspheres deposited in the non-lasered regions of the TM, suggesting that aqueous humor primarily exits the anterior chamber via these non-lasered regions (Melamed and Epstein, 1987; Zhang et al., 2009). In contrast, few to no fluorescent tracers were found in regions of the TM treated with laser photocoagulation, suggesting scant egress of aqueous humor through these regions. The current study perfused fluorescein dye to label the episcleral veins (ESVs) and thereby identify lasered and non-lasered regions of outflow in this model. Unlasered, normotensive control eyes were similarly perfused to evaluate morphological differences between high-flow and low-flow regions. This was done, because studies of humans (Cha et al., 2016; Hann et al., 2005) and monkeys (Lu et al., 2011; Sabanay et al., 2000) have demonstrated segmental outflow via the conventional outflow

Author Manuscript Author Manuscript Author Manuscript Author Manuscript

pathway in normal eyes. Additionally, the segmental nature of aqueous humor outflow is conserved past the proximal trabecular outflow pathway to the level of the ESVs (Cha et al., 2016). The goal was to study morphological changes in the proximal and distal outflow pathways in a monkey model of laser-induced ocular hypertension between regions of variable aqueous humor outflow.

2. Materials and Methods

2.1. Animals, Laser treatment, and IOP

This study examined the eyes of seven adult female cynomolgus macaques. One eye of six monkeys and both eyes of one monkey were treated with Nd:YAG laser photocoagulation (Ophthalas 532 EyeLite Laser, Alcon Laboratories, Inc. 6201 South Freeway, Fort Worth, Texas) of the TM ($n = 8$) under isoflurane anesthesia. Contralateral eyes were untouched and used as normotensive controls ($n = 5$). Fifty to 100 laser photocoagulation burns with a spot size of 50 μm, a power of 1000 mW, and an exposure time of 0.5s were made to approximately 270 to 340 degrees of the TM. Within 3 months of the first laser procedure, treatments were repeated one to two more times with one month recovery between treatments. No further lasering was ever done. Persistent IOP elevation was noted in all but one laser-treated eye following treatment. The remaining TM (approximately 20–90 degrees) was left untreated. The reported IOPs were measured by pneumotonometry (Model 30; Reichert, Inc., Depew, NY) at two time points. Intermediate IOPs were measured at 10–48 prior to final IOPs and final IOPs were measured at 60–182 months following the last laser treatment (Table 1). Six monkeys were used in unrelated drug trials utilizing nitric oxide donors, endothelin receptor antagonists, and selective EP2 receptor agonists following laser treatment. Five monkeys had a wash out period following drug trials of at least 3 months, while one monkey had a washout period of less than one month prior to euthanasia. Monkeys were euthanized between 58 and 183 months after their last laser treatment (mean ± SEM; 152.6 ± 14.7 months), and eyes were sent to Boston University within 24 hours of enucleation. All experimental procedures were approved by the Institutional Animal Care and Use Committee of the University of Nebraska Medical Center and Covance Laboratories, Inc. (Madison,WI), and were implemented in accordance with the ARVO Statement for the Use of Animals in Ophthalmic and Vision Research.

2.2. Ocular perfusion

All eyes ($n = 8$ laser-treated and $n = 5$ controls) were perfused at 15 mmHg with Dulbecco's phosphate-buffered saline (DPBS) (Life Technologies, Grand Island, NY, USA) containing 5.5mM of D-glucose (GPBS) for 30 min to establish baseline outflow facility. One control eye was excluded from the study as the outflow facility was noted to be abnormally elevated and a leak in the globe was suspected. To visualize the outflow pattern, anterior chambers of laser-treated eyes ($n = 5$) and control eyes ($n = 2$) received later in the study were exchanged and perfused with fluorescein (0.1%, Sigma-Aldrich) in GPBS for 10 minutes. Eyes were illuminated using cobalt blue light and imaged once episcleral veins displayed fluorescence to document segmental outflow (~3 minutes after perfusion resumed after exchange) (Fig. 1). Regions displaying fluorescence were considered high-flow, and regions without fluorescence were considered low-flow. It is worth noting that previous studies

Author Manuscript Author Manuscript Author Manuscript Author Manuscript

evaluating outflow patterns examined indicators of outflow at the level of the TM, SC, and ESV (Cha et al., 2016) whereas in the current study, we evaluated outflow solely at the level of the ESVs by perfusion of fluorescent dye (Huang et al., 2017, 2016). While the segmental pattern of outflow was conserved distally, ESVs do not project radially from a corresponding region of TM (Cha et al., 2016). For this reason, we considered adjacent regions of the proximal outflow pathway as low-flow as opposed to non-flow, as minimal fluorescence in adjacent ESVs may not be an exact representation of outflow status of more proximal regions of the outflow pathway in the same clock hour. Anterior chambers of all eyes were exchanged and perfused at the same pressure for 1 hour with 1% glutaraldehyde and 4% paraformaldehyde in DPBS containing 30 mmol/L $MgCl_2$ and 0.05% (w/v) Alcian Blue 8GX. Alcian Blue 8GX was used for a separate study of the glycocalyx at the electron microscopic level. All eyes were hemisected and immersion-fixed in the same solution overnight.

2.3. Light and Electron Microscopy

Anterior segments of each eye were dissected into 24 to 36 radial wedges. Wedges were post-fixed with 1% aqueous osmium tetroxide and 1% lanthanum (III) nitrate hydrate at room temperature for 2 hours, *en-bloc* stained with 1.5% uranyl acetate, and dehydrated in a graded series of ethanols. Wedges were infiltrated with propylene oxide and embedded in 100% epon-araldite. Semi-thin (2 μm) sections were cut and stained with 1% toluidine blue. Three or more sections were examined for each eye via light microscopy and images of the trabecular outflow pathway were collected at an objective magnification of 20X and 40X to evaluate the morphology of SC and the intrascleral veins (ISVs) in lasered and non-lasered regions of laser-treated eyes and in high-flow and low-flow regions of control eyes. Cross-sectional area (CSA) (Fig. 2A), mean height per section (Fig. 2B), and anterior-to-posterior width of SC (Fig. 2C) were measured and compared between high-flow and low-flow regions of control eyes, as well as between non-lasered regions of laser-treated eyes and control eyes. SC was partially or completely obliterated in lasered regions of laser-treated eyes and could not be quantitatively evaluated. Number and CSA (Fig. 2D) of ISVs within 600 μm posterior to SC were evaluated between lasered and non-lasered regions of laser-treated eyes and control eyes, as well as between high-flow and low-flow regions of control eyes. All measurements were completed using ImageJ (Version 1.53g, National Institutes of Health). Upon light microscopic evaluation, remodeling of the sclera in lasered sections prompted examination of the sclera across all groups via electron microscopy to compare scleral composition and organization. Ultra-thin (70–80 nm) sections were cut and examined via transmission electron microcopy. Measurements of 100 collagen fibril diameters were performed per eye from ≥ 2 images taken within the sclera < 80 μm from the outer wall of SC from control, lasered, and non-lasered regions. Measurements of collagen fibril density (fibrils/μm^2) were performed in four randomly selected regions (0.8 μm × 0.6 μm) of ≥ 2 images per eye. These images were taken within the sclera < 80 μm from the outer wall of SC from control, lasered, and non-lasered regions.

2.4. Statistical Methods

All statistical analyses were performed using R statistical computing package (v3.5.1; R Foundation for Statistical Computing, Vienna, Austria). All data are listed as median and

Author Manuscript Author Manuscript Author Manuscript Author Manuscript

interquartile range. IOP and outflow facility were compared between laser-treated and control eyes using Wilcoxon rank-sum tests. Number and CSA of ISVs were averaged by eye and Kruskal-Wallis tests with *post-hoc* pairwise Wilcoxon rank-sum tests were used to test for statistical significance between control, lasered, and non-lasered regions. As only two control eyes were perfused with fluorescein, data between high- and low-flow control regions were not averaged by eye. Kolmogorov-Smirnov (KS) tests, which were used to assess the normality of the data distributions, demonstrated non-normal distributions ($P < 0.01$). Therefore, data were listed as median and interquartile range, and Wilcoxon rank-sum tests were used to assess statistical significance. SC parameters, including anterior to posterior width, height, and CSA of SC, were averaged by eye and compared between control and non-lasered regions using Wilcoxon rank-sum tests. In comparing the aforementioned SC parameters between high- and low-flow regions of control eyes, KS tests showed non-normal distributions ($P < 0.01$), and thus, data were reported as median and interquartile range and assessed by Wilcoxon rank-sum tests. Scleral collagen fibril diameters were averaged by eye, compared between control, lasered, and non-lasered regions, and assessed by Kruskal-Wallis tests with *post-hoc* pairwise Wilcoxon rank-sum tests. Scleral collagen densities were averaged by eye and compared between control, lasered, and non-lasered regions, and assessed by Kruskal-Wallis tests with *post-hoc* pairwise Wilcoxon rank-sum tests. A subset of all measurements was repeated after at least one week, and the difference between the initial and subsequent measurements was < 10% for all parameters.

3. Results

3.1. Intraocular pressure

Median final IOP was greater in laser-treated eyes (28.65 mmHg, IQR: 24.28 – 31.08; n = 8) compared to control eyes (22.00 mmHg, IQR: 22.00 – 27.50; $n = 5$), but this difference was not statistically significant ($P = 0.38$; Fig. 3A). Median intermediate IOP was significantly greater in laser-treated eyes (34.50 mmHg, IQR: 29.45 – 35.2; n = 7) compared to control eyes (25.1 mmHg, IQR: 23.28 – 27.75; n = 4; $P = 0.04$; Table 1).

3.2. Outflow Facility

Median outflow facility was significantly decreased in laser-treated eyes (0.08 μL/min/mmHg, IQR: 0.03 – 0.17; $n = 8$) compared to control eyes (0.33, IQR: 0.30 – 0.48; $n = 5$; $P = 0.02$; Fig. 3B).

3.3. Light microscopy

3.3.1 TM, SC, and Collector Channels—In control eyes (Fig. 4A), SC was partially or fully open, the TM displayed wide intertrabecular spaces (ITSs), and patent collector channel (CC) ostia were common. In non-lasered regions of laser-treated eyes, the TM, SC, and CCs appeared similar to control eyes (Fig. 4B). The TM displayed discrete beams with prominent ITSs, SC was notably patent with variable contact between the inner and outer walls, and CC ostia were prominent in multiple sections. In lasered regions of laser-treated eyes (Fig. 4C), dense, pigmented TM with condensed or collapsed ITSs was common. SC was frequently partially or completely obliterated, and CC ostia could not be definitively

Author Manuscript Author Manuscript Author Manuscript Author Manuscript

identified. Therefore, measurements of SC were limited to control eyes and non-lasered regions of laser-treated eyes. Upon comparing the high- and low-flow regions of control eyes qualitatively, high-flow regions (Fig. 5A) typically had more expansive JCT with more narrowing and partial collapse of SC, compared to low-flow regions of control eyes (Fig. 5B). A significantly smaller median CSA (810 μm^2, IQR: 680 – 900 vs 1340 μm^2, IQR: 880 – 1910; $n = 8$; $P = 0.01$, Fig. 5C) and average height (3.6 μm, IQR: 1.3 – 4.8 vs 6.7 μm, IQR: 4.3 – 8.5; $n = 8$; $P = 0.04$, Fig. 5D) of SC were found in high-flow regions compared to low-flow regions of control eyes. Anterior-to-posterior width of SC did not differ significantly between high-flow (264 μm, IQR: 244 – 327; $n = 8$) and low-flow (249 μm, IQR: 214 – 251; $n = 8$; $P = 0.19$) control regions. However, when high- and low-flow regions of control eyes were evaluated as a whole, the median CSA (1707 μm^2, IQR 801 – 1899; $n = 5$), average height (3.9 μm, IQR: 3.8 – 5.7; $n = 5$), and anterior-to-posterior width (273 μm, IQR: 256 – 302; $n = 5$) of SC in control eyes were not significantly different from the median CSA (1188 μm^2, IQR: 878 – 2300; $n = 6$; $P = 0.66$; Fig. 6A), height (5.9 μm, IQR: 2.8 – 7.2; $n = 6$; $P = 0.93$; Fig. 6B), and anterior-to-posterior width (289 μm, IQR: 276 – 319; $n = 6$; $P = 0.43$; Fig. 6C), of non-lasered regions of laser-treated eyes.

3.3.2 Intrascleral Veins—ISV number and CSA were evaluated between lasered and non-lasered regions of laser-treated eyes and control eyes, and between high-flow and low-flow regions of control eyes. ISVs within a predetermined distance posterior to SC were included for analysis. ISVs with a ratio between their major and minor axes of greater than 10 were excluded from consideration, because they were considered oblique sections. The median number of ISVs per mm sclera was significantly different between lasered, non-lasered, and control regions (Kruskal-Wallis test, $P < 0.01$; Fig. 7). Specifically, the median number of ISVs per mm sclera was significantly lower in lasered regions of laser-treated eyes (1.5 ISV/mm, IQR: 0.7 – 2.2; $n = 8$) than in non-lasered regions of laser-treated eyes (3.7 ISV/mm, IQR: 3.3 – 4.3; $n = 6$; $P < 0.01$; Table 2) and control eyes (5.7 ISV/mm, IQR: 4.2 – 6.3; $n = 5$; $P < 0.01$). The median number of ISVs per mm sclera was not significantly different between non-lasered regions of laser-treated eyes and control eyes ($P = 0.25$) or between high-flow (4.7 ISVs/mm, IQR: 3.6 – 5.6; $n = 8$) and low-flow (5.9 ISVs/mm, IQR: 4.7 – 7.6; $n = 8$; $P = 0.33$) regions of control eyes. Median ISV CSA in control eyes (135 μm^2, IQR: 132 – 142; $n = 5$), lasered (60 μm^2, IQR: 38 – 137; $n = 7$), and non-lasered regions (188 μm^2, IQR: 179 – 236; $n = 6$) of lasered eyes did not differ significantly (Kruskal-Wallis test, $P = 0.16$; Table 2). In addition, there was no significant difference in median ISV CSA between high-flow (86 μm^2, IQR: 51 – 187; $n = 34$) and low-flow (54 μm^2, IQR: 35 – 130; $n = 39$; $P = 0.21$) regions of control eyes.

The sclera adjacent to the TM in many laser-treated regions appeared less compact and more disorganized than that of non-lasered regions and control eyes (Fig. 7A–C). This change was further investigated using electron microscopy.

3.4. Electron microscopy

Median scleral collagen fibril diameters from sclera adjacent to the TM in controls, lasered, and non-lasered regions of lasered eyes were 67, 49, and 75 nm, respectively, which were significantly different (Kruskal-Wallis test, $P = 0.02$). Specifically, collagen fibrils in lasered

Author Manuscript Author Manuscript Author Manuscript Author Manuscript

regions (49 nm, IQR: 45 – 55; $n = 8$) were significantly smaller than in non-lasered regions (75 nm, IQR: 64 – 82; $n = 6$; $P = 0.02$) of lasered eyes and controls (67 nm, IQR: 65 – 78; $n = 5$; $P = 0.03$; Fig. 8). Collagen fibril diameter did not differ significantly between control and non-lasered regions ($P = 0.79$). In addition, while control and non-lasered regions displayed uniform toluidine blue staining of the sclera, lasered regions displayed lightly stained regions of sclera, which corresponded with regions of increased open spaces between collagen fibril bundles upon electron microscopic evaluation (Fig. 9). Median collagen fibril densities from the sclera adjacent to the TM in control, lasered, and non-lasered regions of lasered eyes were 94.8, 71.6, and 24.9 fibrils/μm^2, respectively, which were significantly different (Kruskal-Wallis test, $P < 0.01$). Specifically, collagen fibril density was decreased in lasered regions (24.9 fibrils/μm^2, IQR: 22.8 – 37.8; $n = 8$) compared to both control (94.8 fibrils/μm^2, IQR: 90.9 – 104.0; $n = 5$; $P < 0.01$) and non-lasered regions (71.6 fibrils/μm^2, IQR: 68.3 – 91.1; $n = 6$; $P < 0.01$; Fig. 10). Collagen fibril density did not differ significantly between control and non-lasered regions ($P = 0.25$).

4. Discussion

Morphological changes in the proximal and distal conventional outflow pathway found in this study include: 1) collapse of ITSs of the TM, 2) collapse of SC and CCs, and 3) decreased number of patent ISVs in laser-treated regions. These morphological changes may have contributed to the significantly decreased outflow facility in laser-treated eyes and support the existence of increased outflow resistance in a model of laser-induced ocular hypertension in cynomolgus macaques.

The coagulative effects of laser treatment on the TM, subsequent TM scarring and pigment accumulation, ITS collapse, and collapse of SC have been well documented in both humans with POAG (Babizhayev et al., 1990; Wise and Witter, 1979) and monkeys (Gaasterland and Kupfer, 1974; Melamed et al., 1985; Melamed and Epstein, 1987; Zhang et al., 2009). There is little to no aqueous humor outflow in lasered regions of the TM. Instead, aqueous humor flows through adjacent non-lasered regions of the TM (Melamed and Epstein, 1987; Zhang et al., 2009). Global imaging with fluorescein perfusion in our study was similarly indicative that aqueous humor primarily exits through non-lasered regions of the TM. These non-lasered regions, in contrast to lasered regions, displayed wide ITSs, an expansive JCT, and partial or complete patency of SC and CCs (Fig. 4B). Laser-induced changes to the TM, SC, and CCs clearly play a significant role in increasing outflow resistance and reducing active outflow areas.

Although no significant difference was observed in the TM and SC dimensions between the non-lasered regions of laser-treated eyes and control eyes, we observed a more expansive JCT with reduced CSA and height of SC in high-flow regions (Fig. 5A) compared to low-flow regions of control eyes (Fig. 5B). These observations are consistent with previous findings of high-flow and low-flow regions in normal human (Cha et al., 2016; Hann et al., 2005) and monkey eyes (Zhang et al., 2009). Expansion of the JCT may lower the outflow resistance and increase the active outflow in these regions (Melamed and Epstein, 1987; Yang et al, 2013; Ren et al, 2016).

Author Manuscript Author Manuscript Author Manuscript Author Manuscript

While numerous studies have evaluated outflow resistance of the proximal outflow pathway in both experimental animal models and clinical POAG eyes, changes in the distal outflow pathway and their contributions to outflow resistance have not been thoroughly evaluated. The distal outflow pathway may account for 30–50% of outflow resistance, and multiple studies evaluating the properties and function of vessels distal to SC have indicated potential means of resistance modulation (Grant, 1963; Rosenquist et al., 1989; Schuman et al., 1999). Vessels within the distal outflow pathway, including ISVs, contain α-smooth muscle actin, suggesting they may have contractile properties and the potential to modulate outflow resistance (de Kater et al., 1992; Gonzalez et al., 2017; Selbach et al., 2005). Interestingly, these vessels can be regulated pharmacologically. Cromakalim, a potassium channel opener, lowers IOP in trabeculotomized human eyes (Chowdhury et al., 2017). One of the mechanisms by which Netarsudil, a rho kinase/norepinephrine transporter inhibitor, increases outflow facility in human eyes is through dilation of ESVs, although its effects on ISVs have yet to be explored (Ren et al., 2016).

Not only are these vessels subject to pharmacologic regulation, but they are influenced by physiologic vasoregulators as well. Nitric oxide, a vasodilator, and endothelin-1, a vasoconstrictor, can cause significant shifts in outflow facility in trabeculotomized human eyes, suggesting not only that the vessels of the distal outflow pathway are subject to vasoregulation, but also that this vasoregulation can have a significant impact on outflow resistance (McDonnell et al., 2018; Waxman et al., 2018). Interestingly, in our study, there were fewer patent ISVs in the lasered regions of laser-treated eyes than non-lasered regions or control eyes. We hypothesize that collapse of some ISVs may have occurred, contributing to increased outflow resistance and decreased outflow facility; however, whether the collapse may be attributed to physiologic vasoconstrictors or a mechanical response to decreased flow through more proximal components of the outflow pathway requires further investigation. Given the documented role of ISVs in resistance modulation and their susceptibility to pharmacologic intervention, our findings suggest ISVs may be a potential target for glaucoma treatment. Surprisingly, while laser-treated regions had smaller median ISV CSAs than controls and non-laser treated regions, this difference was not statistically significant. One explanation might be that smaller diameter vessels were more likely to collapse completely, so we did not measure them, and thus, the median CSA of the remaining measurable vessels in the laser-treated region was closer to that of the controls.

This study also found scleral remodeling adjacent to laser-treated regions of the TM (Fig. 9). Evaluation of the sclera via light microscopy revealed scleral remodeling characterized by tissue rarefication and a more loosely organized scleral stroma in select lasered regions alone. Further investigation of these regions via electron microscopy revealed a decreased median collagen fibril diameter and regions of decreased collagen fibril density. To our knowledge, these changes have not previously been reported in the experimental monkey model of laser-induced ocular hypertension.

Interestingly, these changes were not observed in the sclera adjacent to non-lasered regions in laser-treated eyes, which strongly suggests these are biological or mechanical changes incited by laser photocoagulation of the TM. The decreases in collagen fibril size and density may reflect increased synthesis of small diameter fibrils or selective degradation of

Author Manuscript Author Manuscript Author Manuscript Author Manuscript

larger diameter collagen fibrils. We speculate that thermal energy from laser trabeculoplasty may stimulate induction of matrix metalloproteinases (Kagan et al., 2014; Parshley et al., 1996), which regulate synthesis and degradation of scleral collagen and associated matrix proteoglycans. These proteoglycans play a critical role in fibrillogenesis and modulation of fibril size, orientation, and arrangement (Austin et al., 2002; Chakravarti et al., 2003; Ouyang et al., 2019; Rada et al., 1993; Vogel et al., 1984). Conceivably, thermal energy utilized in coagulation of the TM in our model may have had a similar effect on the adjacent scleral tissue, inducing matrix metalloproteinases, and thereby altering extracellular matrix composition and collagen fibrillogenesis and degradation. Direct thermal injury would be less likely, because the typical short-term response of collagen fibrils to thermal stress is cross-sectional enlargement (Rem et al., 2001). The morphological changes that occur over a longer period of time, such as those of our study, have not been thoroughly explored. However, given the long-term nature of our study, it is unclear at this time whether the morphological changes noted occurred immediately after laser treatment, or over a longer time course and thus possible causes of these changes require further investigation.

Another possible cause of a decrease in median collagen fibril diameter may be thinning of fibrils secondary to increased strain (Rigozzi et al., 2011). Coagulation and subsequent scarring of the TM may have changed the mechanical relationship with the adjacent sclera, altering tension on those fibrils, and thereby affecting diameter. However, it must be stressed that at this time this hypothesis is only conjecture. Whether changes in scleral collagen fibril diameter and density in laser-treated regions of this model resulted from altered scleral extracellular matrix biochemistry or mechanical interactions of fibrils with adjacent structures requires further investigation. A previous study of aqueous humor dynamics utilizing monkeys with laser-induced glaucoma found a significant increase in uveoscleral outflow in laser-treated eyes at least 1 year following treatment (Toris et al., 2000). Whether the regions of tissue rarefication within the scleral stroma in this study may contribute to an increase in uveoscleral outflow in this model merits closer scrutiny.

In this study, median IOP was significantly greater in laser-treated eyes (34.50 mmHg, IQR: 29.45 – 35.2; n = 7) compared to control eyes (25.1 mmHg, IQR: 23.28 – 27.75; n = 4; Wilcoxon rank sum: $P = 0.04$) when comparing values measured 10–48 months prior to the final IOP measurements reported in this study. Our reported final median IOP was greater in laser-treated eyes compared to controls, but this difference was not statistically significant. IOPs in this study were similar to IOPs reported in previous studies utilizing this model in cynomolgus macaques (Miyahara et al., 2003; Raghunathan et al., 2017). While IOP in one animal did not reach persistently elevated levels following laser-treatment (Animal 6, OS), outflow facility was significantly decreased in this eye (0.04 μL/min/mmHg) and the eye displayed morphological changes similar to all other laser-treated eyes, therefore it was included in analysis. A multiple regression analysis was performed to analyze the effects that the variables of SC CSA, SC height, SC width, ISV number, scleral fibril diameter, and scleral fibril density have on the final IOP of the two groups of monkey eyes. We did not find a significant correlation between IOP and any of these parameters when accounting for group ($P = 0.67$). However, it must be stressed that glaucoma is a complex, multi-factorial disease, and several factors unassessed in this study may have come into effect, including the potential increase in uveal outflow in lasered eyes (Toris and Pederson, 1985). In addition,

Author Manuscript Author Manuscript Author Manuscript Author Manuscript

the ocular hypertensive eyes had IOPs that fluctuated greatly compared to control eyes, and due to the high variability and standard deviation, the IOPs were not statistically different from the control eyes at the time of final IOP measurement. As we have noted, these animals had significantly higher intermediate IOPs in lasered eyes than in control eyes (Table 1). Similarly, glaucoma patients often have more fluctuations in IOP compared to healthy age-matched controls (Drance, 1960). However, median outflow facility was significantly decreased in laser-treated eyes compared to control eyes, suggesting uveal outflow facility may be increased in the lasered eyes, which is consistent with a previous report in this model (Toris et al., 2000).

One limitation of this study was the small sample size of control eyes perfused with fluorescein. A comparison of morphological characteristics of the outflow pathway between non-lasered regions and low-flow and high-flow regions of control eyes individually would be of interest in the future. As aqueous humor exits the anterior chamber in laser-treated eyes primarily via non-lasered regions of the trabecular meshwork, we would expect to see more morphological similarities in these regions with high-flow regions than low-flow regions of control eyes. In addition, as this was a histologic study, factors such as tissue fixation must be considered when attempting to compare these findings to what may be expected *in vivo.*

While collapse of the TM and partial to complete obliteration of SC increased outflow resistance in previous studies of the laser-induced model of non-human primate ocular hypertension, our study further investigated possible contributing sources of distal resistance. In this study, a decrease in the number of patent ISVs was found in laser-treated regions, suggesting that the lack of these vessels contributes to the decrease in outflow facility observed in this model. In addition, scleral remodeling following laser-treatment may impact outflow, though the exact cause and effect of the changes in scleral composition require further investigation. Overall, our results suggest that the distal outflow pathway modulates outflow resistance and could represent a potential therapeutic target for IOP regulation in POAG.

Acknowledgements

We are grateful to our funding sources: NIH grants EY022634 (HG), EY028674 (HG), EY030318 (DLS), and and S10OD028571, The Rifkin Family Glaucoma Research Fund (HG), and The Massachusetts Lions Eye Research Fund (HG). We also thank Eva Ho and Dr. Chen-Yuan Charlie Yang for their technical assistance.

Abbreviations:

CC	collector channel
CSA	cross-sectional area
DPBS	Dulbecco’s phosphate-buffered saline
ESV	episcleral vein
GPBS	Dulbecco’s phosphate-buffered saline containing 5.5mM of D-glucose

Author Manuscript Author Manuscript Author Manuscript Author Manuscript

IOP	intraocular pressure
ITS	intertrabecular space
ISV	intrascleral vein
JCT	juxtacanalicular connective tissue
KS	Kolmogorov-Smirnov
POAG	primary open-angle glaucoma
SC	Schlemm's canal
TM	trabecular meshwork

References

The Advanced Glaucoma Intervention Study (AGIS): 7. The relationship between control of intraocular pressure and visual field deterioration.The AGIS Investigators., 2000. . Am. J. Ophthalmol. 130, 429–440. 10.1016/s0002-9394(00)00538-9 [PubMed: 11024415]

Arriola-Villalobos P, Martínez-de-la-Casa JM, Díaz-Valle D, Fernández-Pérez C, GarcíaSánchez J, García-Feijoó J, 2012. Combined iStent trabecular micro-bypass stent implantation and phacoemulsification for coexistent open-angle glaucoma and cataract: a long-term study. Br. J. Ophthalmol. 96, 645–649. 10.1136/bjophthalmol-2011-300218 [PubMed: 22275344]

Austin BA, Coulon C, Liu C-Y, Kao WW-Y, Rada JA, 2002. Altered collagen fibril formation in the sclera of lumican-deficient mice. Invest. Ophthalmol. Vis. Sci. 43, 1695–1701. [PubMed: 12036967]

Babizhayev MA, Brodskaya MW, Mamedov NG, YYe B, 1990. Clinical, structural and molecular phototherapy effects of laser irradiation on the trabecular meshwork of human glaucomatous eyes. Graefe's Arch. Clin. Exp. Ophthalmol. = Albr. von Graefes Arch. fur Klin. und Exp. Ophthalmol. 228, 90–100. 10.1007/BF02764299

Bill A, 1966. Conventional and uveo-scleral drainage of aqueous humour in the cynomolgus monkey (Macaca irus) at normal and high intraocular pressures. Exp. Eye Res. 5, 45–54. 10.1016/s0014-4835(66)80019-2 [PubMed: 4160221]

Cha EDK, Xu J, Gong L, Gong H, 2016. Variations in active outflow along the trabecular outflow pathway. Exp. Eye Res. 146, 354–360. 10.1016/j.exer.2016.01.008 [PubMed: 26775054]

Chakravarti S, Paul J, Roberts L, Chervoneva I, Oldberg A, Birk DE, 2003. Ocular and scleral alterations in gene-targeted lumican-fibromodulin double-null mice. Invest. Ophthalmol. Vis. Sci. 44, 2422–2432. 10.1167/iovs.02-0783 [PubMed: 12766039]

Chowdhury UR, Rinkoski TA, Bahler CK, Millar JC, Bertrand JA, Holman BH, Sherwood JM, Overby DR, Stoltz KL, Dosa PI, Fautsch MP, 2017. Effect of Cromakalim Prodrug 1 (CKLP1) on Aqueous Humor Dynamics and Feasibility of Combination Therapy With Existing Ocular Hypotensive Agents. Invest. Ophthalmol. Vis. Sci. 58, 5731–5742. 10.1167/iovs.17-22538 [PubMed: 29114841]

de Kater AW, Shahsafaei A, Epstein DL, 1992. Localization of smooth muscle and nonmuscle actin isoforms in the human aqueous outflow pathway. Invest. Ophthalmol. Vis. Sci. 33, 424–429. [PubMed: 1740375]

Drance SM, 1960. The significance of the diurnal tension variations in normal and glaucomatous eyes. Arch. Ophthalmol. (Chicago, Ill. 1960) 64, 494–501. 10.1001/archopht.1960.01840010496004 [PubMed: 13724271]

Gaasterland D, Kupfer C, 1974. Experimental glaucoma in the rhesus monkey. Invest. Ophthalmol. 13, 455–457. [PubMed: 4208801]

Gonzalez JMJ, Ko MK, Hong Y-K, Weigert R, Tan JCH, 2017. Deep tissue analysis of distal aqueous drainage structures and contractile features. Sci. Rep. 7, 17071. 10.1038/s41598-017-16897-y [PubMed: 29213129]

Author Manuscript Author Manuscript Author Manuscript Author Manuscript

Grant WM, 1963. Experimental aqueous perfusion in enucleated human eyes. Arch. Ophthalmol. (Chicago, Ill. 1960) 69, 783–801. 10.1001/archopht.1963.00960040789022 [PubMed: 13949877]

Hann CR, Bahler CK, Johnson DH, 2005. Cationic ferritin and segmental flow through the trabecular meshwork. Invest. Ophthalmol. Vis. Sci. 46, 1–7. 10.1167/iovs.04-0800 [PubMed: 15623746]

Huang AS, Li M, Yang D, Wang H, Wang N, Weinreb RN, 2017. Aqueous Angiography in Living Nonhuman Primates Shows Segmental, Pulsatile, and Dynamic Angiographic Aqueous Humor Outflow. Ophthalmology 124, 793–803. 10.1016/j.ophtha.2017.01.030 [PubMed: 28237425]

Huang AS, Saraswathy S, Dastiridou A, Begian A, Mohindroo C, Tan JCH, Francis BA, Hinton DR, Weinreb RN, 2016. Aqueous Angiography-Mediated Guidance of Trabecular Bypass Improves Angiographic Outflow in Human Enucleated Eyes. Invest. Ophthalmol. Vis. Sci. 57, 4558–4565. 10.1167/iovs.16-19644 [PubMed: 27588614]

Jea SY, Francis BA, Vakili G, Filippopoulos T, Rhee DJ, 2012. Ab interno trabeculectomy versus trabeculectomy for open-angle glaucoma. Ophthalmology 119, 36–42. 10.1016/j.ophtha.2011.06.046 [PubMed: 21982416]

Johnson M, Shapiro A, Ethier CR, Kamm RD, 1992. Modulation of outflow resistance by the pores of the inner wall endothelium. Invest. Ophthalmol. Vis. Sci. 33, 1670–1675. [PubMed: 1559767]

Kagan DB, Gorfinkel NS, Hutnik CML, 2014. Mechanisms of selective laser trabeculoplasty: a review. Clin. Experiment. Ophthalmol. 42, 675–681. 10.1111/ceo.12281 [PubMed: 24330092]

Kwon YH, Fingert JH, Kuehn MH, Alward WLM, 2009. Primary open-angle glaucoma. N. Engl. J. Med. 360, 1113–1124. 10.1056/NEJMra0804630 [PubMed: 19279343]

Lee PY, Podos SM, Serle JB, Camras CB, Severin CH, 1987. Intraocular pressure effects of multiple doses of drugs applied to glaucomatous monkey eyes. Arch. Ophthalmol. (Chicago, Ill. 1960) 105, 249–252. 10.1001/archopht.1987.01060020103038 [PubMed: 3813959]

Lu Z, Zhang Y, Freddo TF, Gong H, 2011. Similar hydrodynamic and morphological changes in the aqueous humor outflow pathway after washout and Y27632 treatment in monkey eyes. Exp. Eye Res. 93, 397–404. 10.1016/j.exer.2011.05.012 [PubMed: 21669200]

Mäepea O, Bill A, 1992. Pressures in the juxtacanalicular tissue and Schlemm's canal in monkeys. Exp. Eye Res. 54, 879–883. 10.1016/0014-4835(92)90151-h [PubMed: 1521580]

Mäepea O, Bill A, 1989. The pressures in the episcleral veins, Schlemm's canal and the trabecular meshwork in monkeys: effects of changes in intraocular pressure. Exp. Eye Res. 49, 645–663. 10.1016/s0014-4835(89)80060-0 [PubMed: 2806429]

McDonnell F, Dismuke WM, Overby DR, Stamer WD, 2018. Pharmacological regulation of outflow resistance distal to Schlemm's canal. Am. J. Physiol. Cell Physiol. 315, C44–C51. 10.1152/ajpcell.00024.2018 [PubMed: 29631366]

Melamed S, Epstein DL, 1987. Alterations of aqueous humour outflow following argon laser trabeculoplasty in monkeys. Br. J. Ophthalmol. 71, 776–781. 10.1136/bjo.71.10.776 [PubMed: 3676149]

Melamed S, Pei J, Epstein DL, 1985. Short-term effect of argon laser trabeculoplasty in monkeys. Arch. Ophthalmol. (Chicago, Ill. 1960) 103, 1546–1552. 10.1001/archopht.1985.01050100122032 [PubMed: 4051857]

Minckler DS, Baerveldt G, Alfaro MR, Francis BA, 2005. Clinical results with the Trabectome for treatment of open-angle glaucoma. Ophthalmology 112, 962–967. 10.1016/j.ophtha.2004.12.043 [PubMed: 15882909]

Miyahara T, Kikuchi T, Akimoto M, Kurokawa T, Shibuki H, Yoshimura N, 2003. Gene microarray analysis of experimental glaucomatous retina from cynomologous monkey. Invest. Ophthalmol. Vis. Sci. 44, 4347–4356. 10.1167/iovs.02-1032 [PubMed: 14507879]

Ouyang X, Han Y, Xie Y, Wu Y, Guo S, Cheng M, Wang G, 2019. The collagen metabolism affects the scleral mechanical properties in the different processes of scleral remodeling. Biomed. Pharmacother. 118, 109294. 10.1016/j.biopha.2019.109294 [PubMed: 31404770]

Parshley DE, Bradley JM, Fisk A, Hadaegh A, Samples JR, Van Buskirk EM, Acott TS, 1996. Laser trabeculoplasty induces stromelysin expression by trabecular juxtacanalicular cells. Invest. Ophthalmol. Vis. Sci. 37, 795–804. [PubMed: 8603864]

Author Manuscript Author Manuscript Author Manuscript Author Manuscript

Pederson JE, Gaasterland DE, 1984. Laser-induced primate glaucoma. I. Progression of cupping. Arch. Ophthalmol. (Chicago, Ill. 1960) 102, 1689–1692. 10.1001/archopht.1984.01040031373030 [PubMed: 6541902]

Rada JA, Cornuet PK, Hassell JR, 1993. Regulation of corneal collagen fibrillogenesis in vitro by corneal proteoglycan (lumican and decorin) core proteins. Exp. Eye Res. 56, 635–648. 10.1006/exer.1993.1081 [PubMed: 8595806]

Radius RL, Pederson JE, 1984. Laser-induced primate glaucoma. II. Histopathology. Arch. Ophthalmol. (Chicago, Ill. 1960) 102, 1693–1698. 10.1001/archopht.1984.01040031377031 [PubMed: 6541903]

Raghunathan V, Eaton JS, Christian BJ, Morgan JT, Ver Hoeve JN, Yang C-YC, Gong H, Rasmussen CA, Miller PE, Russell P, Nork TM, Murphy CJ, 2017. Biomechanical, ultrastructural, and electrophysiological characterization of the non-human primate experimental glaucoma model. Sci. Rep. 7, 14329. 10.1038/s41598-017-14720-2 [PubMed: 29085025]

Rem AI, Oosterhuis JA, Journée-de Korver HG, van den Berg TJ, Keunen JE, 2001. Temperature dependence of thermal damage to the sclera: exploring the heat tolerance of the sclera for transscleral thermotherapy. Exp. Eye Res. 72, 153–162. 10.1006/exer.2000.0939 [PubMed: 11161731]

Ren R, Li G, Le TD, Kopczynski C, Stamer WD, Gong H, 2016. Netarsudil Increases Outflow Facility in Human Eyes Through Multiple Mechanisms. Invest. Ophthalmol. Vis. Sci. 57, 6197–6209. 10.1167/iovs.16-20189 [PubMed: 27842161]

Rigozzi S, Stemmer A, Müller R, Snedeker JG, 2011. Mechanical response of individual collagen fibrils in loaded tendon as measured by atomic force microscopy. J. Struct. Biol. 176, 9–15. 10.1016/j.jsb.2011.07.002 [PubMed: 21771659]

Rosenquist R, Epstein D, Melamed S, Johnson M, Grant WM, 1989. Outflow resistance of enucleated human eyes at two different perfusion pressures and different extents of trabeculotomy. Curr. Eye Res. 8, 1233–1240. 10.3109/02713688909013902 [PubMed: 2627793]

Sabanay I, Gabelt BT, Tian B, Kaufman PL, Geiger B, 2000. H-7 effects on the structure and fluid conductance of monkey trabecular meshwork. Arch. Ophthalmol. (Chicago, Ill. 1960) 118, 955–962. [PubMed: 10900110]

Schuman JS, Chang W, Wang N, de Kater AW, Allingham RR, 1999. Excimer laser effects on outflow facility and outflow pathway morphology. Invest. Ophthalmol. Vis. Sci. 40, 1676–1680. [PubMed: 10393035]

Selbach JM, Rohen JW, Steuhl K-P, Lütjen-Drecoll E, 2005. Angioarchitecture and innervation of the primate anterior episclera. Curr. Eye Res. 30, 337–344. 10.1080/02713680590934076 [PubMed: 16020264]

Swaminathan SS, Oh D-J, Kang MH, Rhee DJ, 2014. Aqueous outflow: segmental and distal flow. J. Cataract Refract. Surg. 40, 1263–1272. 10.1016/j.jcrs.2014.06.020 [PubMed: 25088623]

Toris CB, Pederson JE, 1985. Effect of intraocular pressure on uveoscleral outflow following cyclodialysis in the monkey eye. Invest. Ophthalmol. Vis. Sci. 26, 1745–1749. [PubMed: 4066210]

Toris CB, Zhan GL, Wang YL, Zhao J, McLaughlin MA, Camras CB, Yablonski ME, 2000. Aqueous humor dynamics in monkeys with laser-induced glaucoma. J. Ocul. Pharmacol. Ther. Off. J. Assoc. Ocul. Pharmacol. Ther. 16, 19–27. 10.1089/jop.2000.16.19

Vahabikashi A, Gelman A, Dong B, Gong L, Cha EDK, Schimmel M, Tamm ER, Perkumas K, Stamer WD, Sun C, Zhang HF, Gong H, Johnson M, 2019. Increased stiffness and flow resistance of the inner wall of Schlemm's canal in glaucomatous human eyes. Proc. Natl. Acad. Sci. U. S. A. 116, 26555–26563. 10.1073/pnas.1911837116

Vogel KG, Paulsson M, Heinegård D, 1984. Specific inhibition of type I and type II collagen fibrillogenesis by the small proteoglycan of tendon. Biochem. J. 223, 587–597. 10.1042/bj2230587 [PubMed: 6439184]

Waxman S, Wang C, Dang Y, Hong Y, Esfandiari H, Shah P, Lathrop KL, Loewen RT, Loewen NA, 2018. Structure-Function Changes of the Porcine Distal Outflow Tract in Response to Nitric Oxide. Invest. Ophthalmol. Vis. Sci. 59, 4886–4895. 10.1167/iovs.18-24943 [PubMed: 30347083]

Weinreb RN, Leung CKS, Crowston JG, Medeiros FA, Friedman DS, Wiggs JL, Martin KR, 2016. Primary open-angle glaucoma. Nat. Rev. Dis. Prim. 10.1038/nrdp.2016.67

Author Manuscript Author Manuscript Author Manuscript Author Manuscript

Wise JB, Witter SL, 1979. Argon laser therapy for open-angle glaucoma. A pilot study. Arch. Ophthalmol. (Chicago, Ill. 1960) 97, 319–322. 10.1001/archopht.1979.01020010165017 [PubMed: 575877]

Yang C-YC, Liu Y, Lu Z, Ren R, Gong H, 2013. Effects of Y27632 on aqueous humor outflow facility with changes in hydrodynamic pattern and morphology in human eyes. Invest. Ophthalmol. Vis. Sci. 54, 5859–5870. 10.1167/iovs.12-10930 [PubMed: 23920374]

Zhang Y, Toris CB, Liu Y, Ye W, Gong H, 2009. Morphological and hydrodynamic correlates in monkey eyes with laser induced glaucoma. Exp. Eye Res. 89, 748–756. 10.1016/j.exer.2009.06.015 [PubMed: 19591828]

Author Manuscript Author Manuscript Author Manuscript Author Manuscript

Highlights

- Studied monkey conventional outflow pathway with laser-induced ocular hypertension
- Schlemm's canal was partially or completely obliterated in laser-treated regions
- Fewer intrascleral veins near meshwork regions treated with laser trabeculoplasty
- Smaller and fewer collagen fibrils in sclera adjacent to laser-treated meshwork
- No difference in Schlemm's canal parameters between non-lasered areas and controls

Author Manuscript Author Manuscript Author Manuscript Author Manuscript

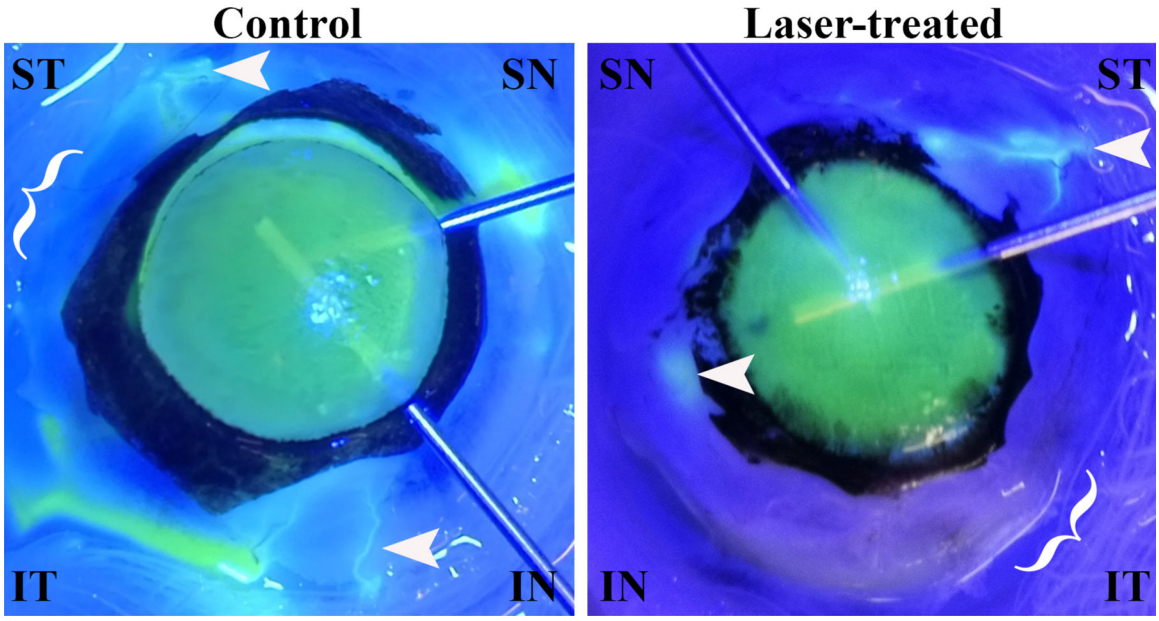

Figure 1.

Segmental flow in control and laser-treated monkey eyes following fluorescein perfusion. *White arrowheads* indicate fluorescent episcleral veins (ESVs), denoting regions of high-flow. *White brackets* demarcate areas without fluorescent ESVs, indicating little to no outflow through the trabecular meshwork (TM) in these regions. IN = inferior nasal; IT = inferior temporal; SN = superior nasal; ST = superior temporal.

Author Manuscript
Author Manuscript
Author Manuscript
Author Manuscript

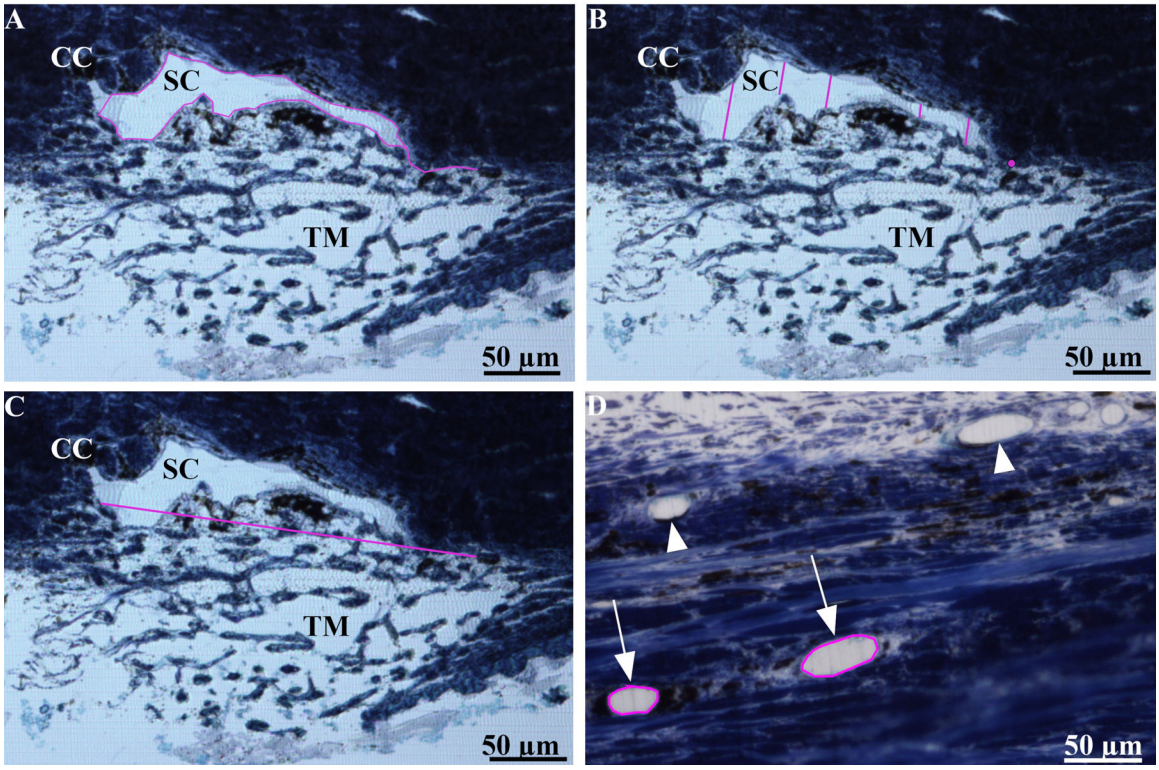

Figure 2.

Methods for measurements using ImageJ. **A:** The measurement for cross-sectional area (CSA) of Schlemm's canal (SC) is indicated by the *magenta outline*. **B:** Height of SC was measured perpendicularly to the inner wall at six consistent points along the anterior-to-posterior width of SC. The average of these six measurements was calculated. *Magenta lines* indicate open regions of SC that were measured. When SC was collapsed (*magenta dot*), height was recorded as 0 µm. **C:** Anterior-to-posterior width of SC is indicated by the *magenta line*. **D:** CSA of intrascleral veins is shown in magenta (*white arrows*). Episcleral veins are indicated by *white arrowheads*. CC = collector channel; TM = trabecular meshwork.

Author Manuscript Author Manuscript Author Manuscript Author Manuscript

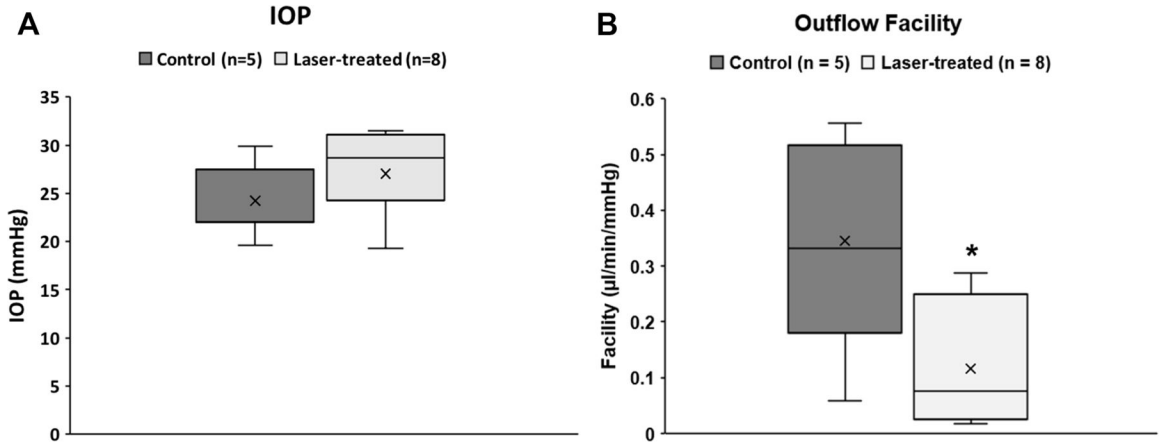

Figure 3.

Intraocular pressure (IOP) and outflow facility. **A:** Median IOP was greater in laser-treated eyes (28.65 mmHg, IQR: 24.28 – 31.08; $n = 8$), compared to control eyes (22 mmHg, IQR: 22.00 – 27.50; $n = 5$), but this difference was not statistically significant ($P = 0.38$). **B:** Outflow facility significantly decreased in laser-treated eyes (0.08 µL/min/mmHg, IQR: 0.03 – 0.17; $n = 8$) compared to normal non-laser-treated controls (0.33, IQR: 0.30 – 0.48; $n = 5$; $P = 0.02$). *Whiskers:* 1.5 interquartile range (IQR). X = mean. * $P < 0.05$.

Author Manuscript Author Manuscript Author Manuscript Author Manuscript

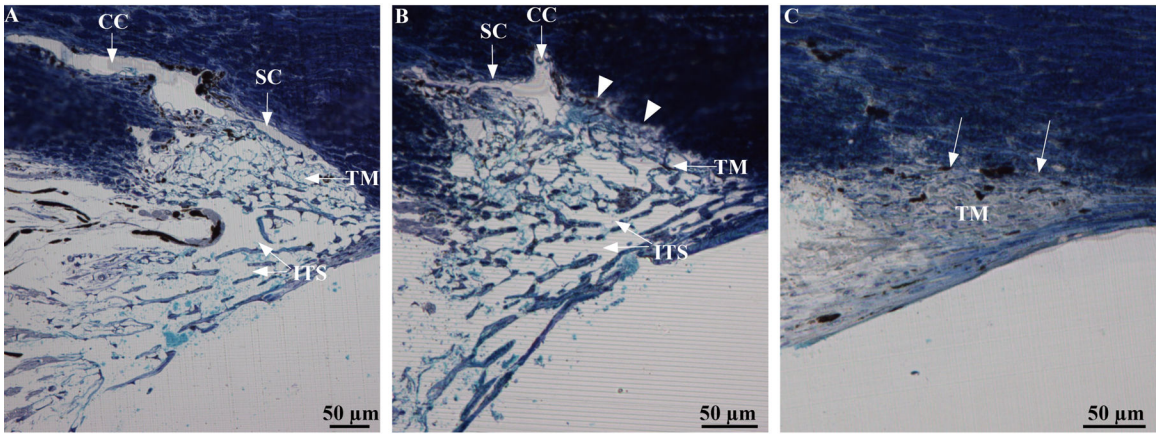

Figure 4.

Light microscopic comparison between control eyes and non-lasered and lasered regions of laser-treated eyes. **A**: In a representative example of control eyes, the trabecular meshwork (TM) appears loose with wide intertrabecular spaces (ITSs), and Schlemm's canal (SC) and a collector channel (CC) appear open. **B**: Similar to control eyes, a representative example of a non-lasered region of a laser-treated eye displays TM with wide ITSs. SC is partially open posteriorly while the inner wall and outer wall are in contact anteriorly (*arrowheads*), and a CC ostium is present. **C**: In a representative example of a lasered region, the TM is condensed with no notable ITSs and some moderate pigment accumulation. SC is obliterated (*small white arrows*), and no CC can be identified.

Author Manuscript Author Manuscript Author Manuscript Author Manuscript

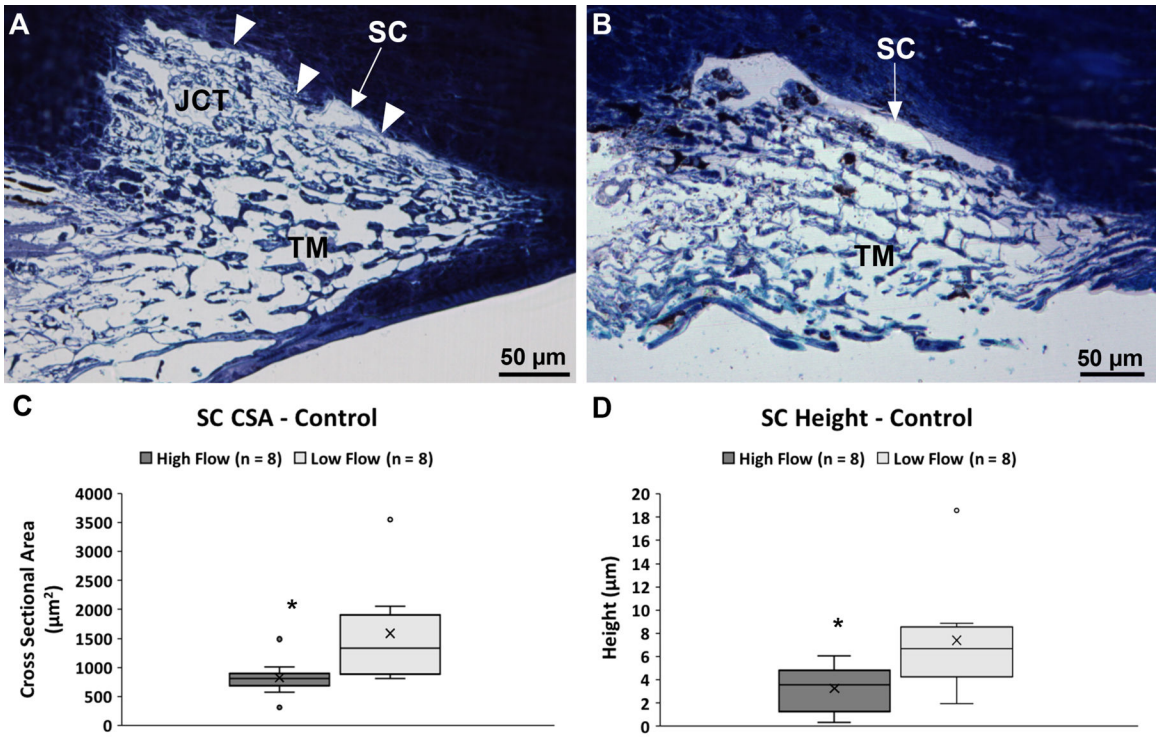

Figure 5.

Schlemm's canal (SC) in control eyes is smaller and narrower in high flow regions compared to low flow regions. **A**: In a representative example of a high flow control region, the juxtacanalicular connective tissue (JCT) is expanded and the inner and outer wall of SC come into contact in multiple locations (*white arrowheads*). **B**: In a representative example of a low flow control region, the JCT is compact, and the lumen of SC is more open compared to the high flow region in **A**. **C**: Median cross-sectional area (CSA) was significantly smaller in high flow regions (810 µm^2, IQR: 680 – 900; $n = 8$) compared to low flow regions (1340 µm^2, IQR: 880 – 1910; $n = 8$; $P = 0.01$) of control eyes. **D**: High flow regions had a significantly smaller height of SC (3.6 µm, IQR: 1.3 – 4.8; $n = 8$) compared to low flow regions (6.7 µm, IQR: 4.3 – 8.5; $n = 8$; $P = 0.04$) of control eyes. *Whiskers:* 1.5 interquartile range (IQR). X = mean. * $P < 0.05$. TM = trabecular meshwork.

Author Manuscript Author Manuscript Author Manuscript Author Manuscript

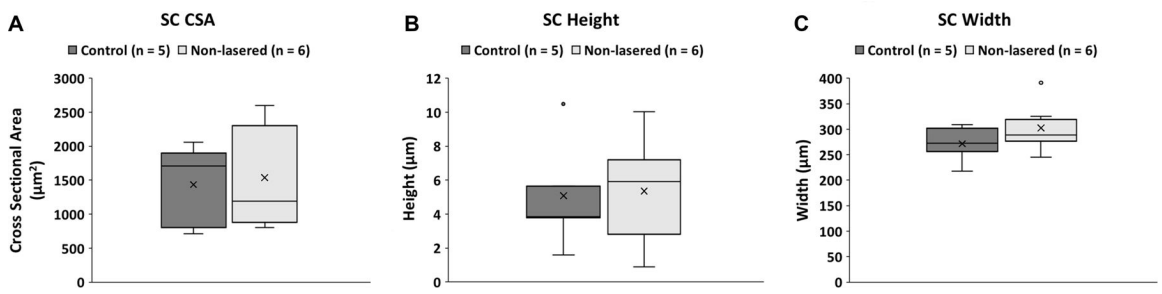

Figure 6.

Comparison of Schlemm's canal (SC) cross-sectional area (CSA), height, and width between control eyes and non-lasered regions of laser-treated eyes. **A**: CSA of SC did not differ significantly between control eyes (1707 μm^2, IQR 801 – 1899; $n = 5$) and non-lasered regions of laser-treated eyes (1188 μm^2, IQR: 878 – 2300; $n = 6$; $P = 0.66$). **B**: Height of SC was not significantly different between control eyes (3.9 μm, IQR: 3.8 – 5.7; $n = 5$) and non-lasered regions of laser-treated eyes (5.9 μm, IQR: 2.8 – 7.2; $n = 6$; $P = 0.93$). **C**: Width of SC did not differ significantly between control eyes (273 μm, IQR: 256 – 302; $n = 5$) and non-lasered regions of laser-treated eyes (289 μm, IQR: 276 – 319; $n = 6$; $P = 0.43$). *Whiskers:* 1.5 interquartile range (IQR). X = mean.

Author Manuscript Author Manuscript Author Manuscript Author Manuscript

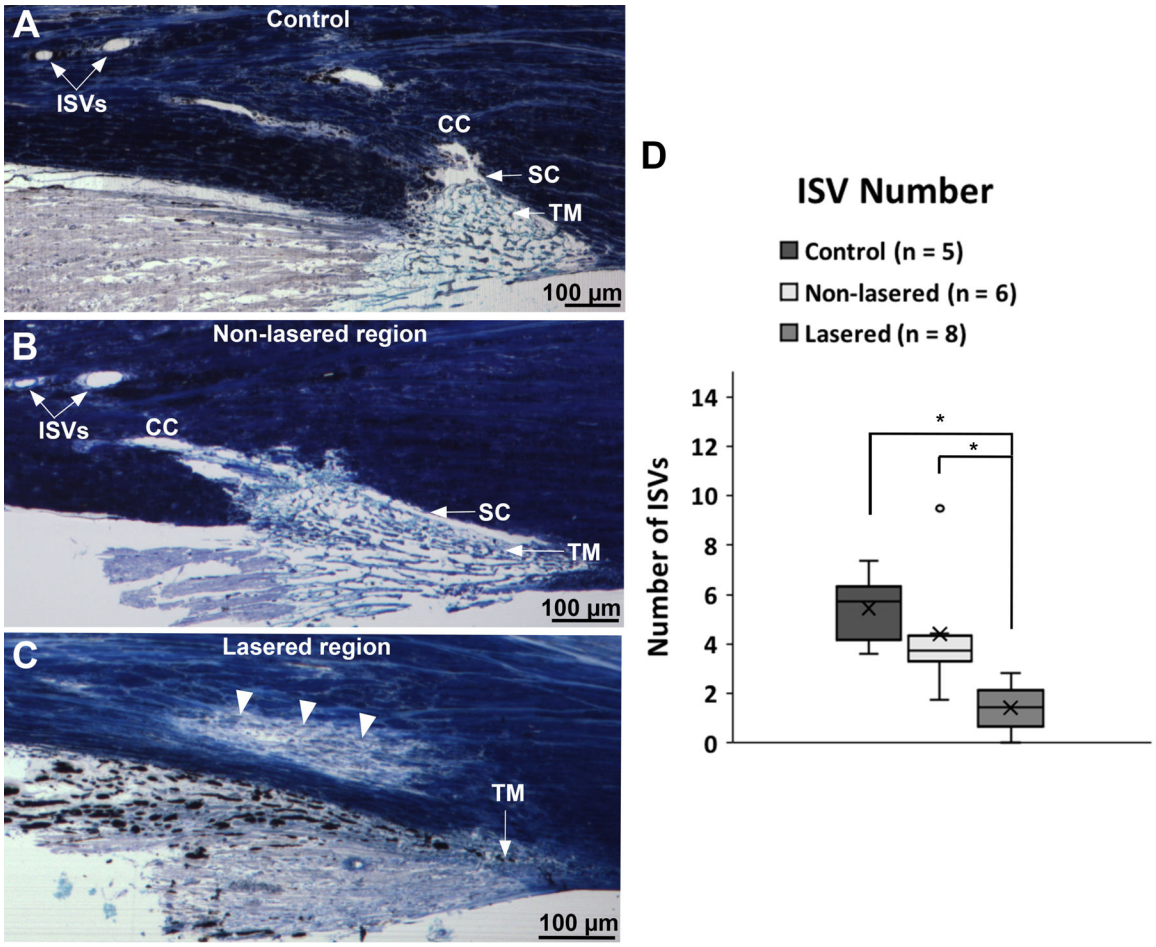

Figure 7.

Comparison of number and cross-sectional area (CSA) of intrascleral veins (ISVs). Control (**A)** and non-lasered regions (**B**) frequently had patent ISVs, whereas lasered regions (**C**) often did not. Sclera adjacent to laser-treated regions of the trabecular meshwork (TM) frequently demonstrated looser and less robustly stained collagen (*white arrowheads* in **C**) than control and non-lasered regions. Laser-treated regions of the TM and adjacent structures frequently displayed significant pigment deposition (**C**). CC = collector channel; SC = Schlemm's canal. **D:** Median ISV number per mm sclera was significantly higher in control eyes (5.7 ISV/mm, IQR: 4.2 – 6.3; $n = 5$; $P < 0.01$), and non-lasered regions (3.7 ISV/mm, IQR: 3.3 – 4.3; $n = 6$; $P < 0.01$), compared to lasered regions (1.5 ISV/mm, IQR: 0.7 – 2.2; $n = 8$). Median CSA of ISVs was not significantly different between groups ($P = 0.16$). *Whiskers:* 1.5 interquartile range (IQR). X = mean. * $P < 0.01$.

Author Manuscript Author Manuscript Author Manuscript Author Manuscript

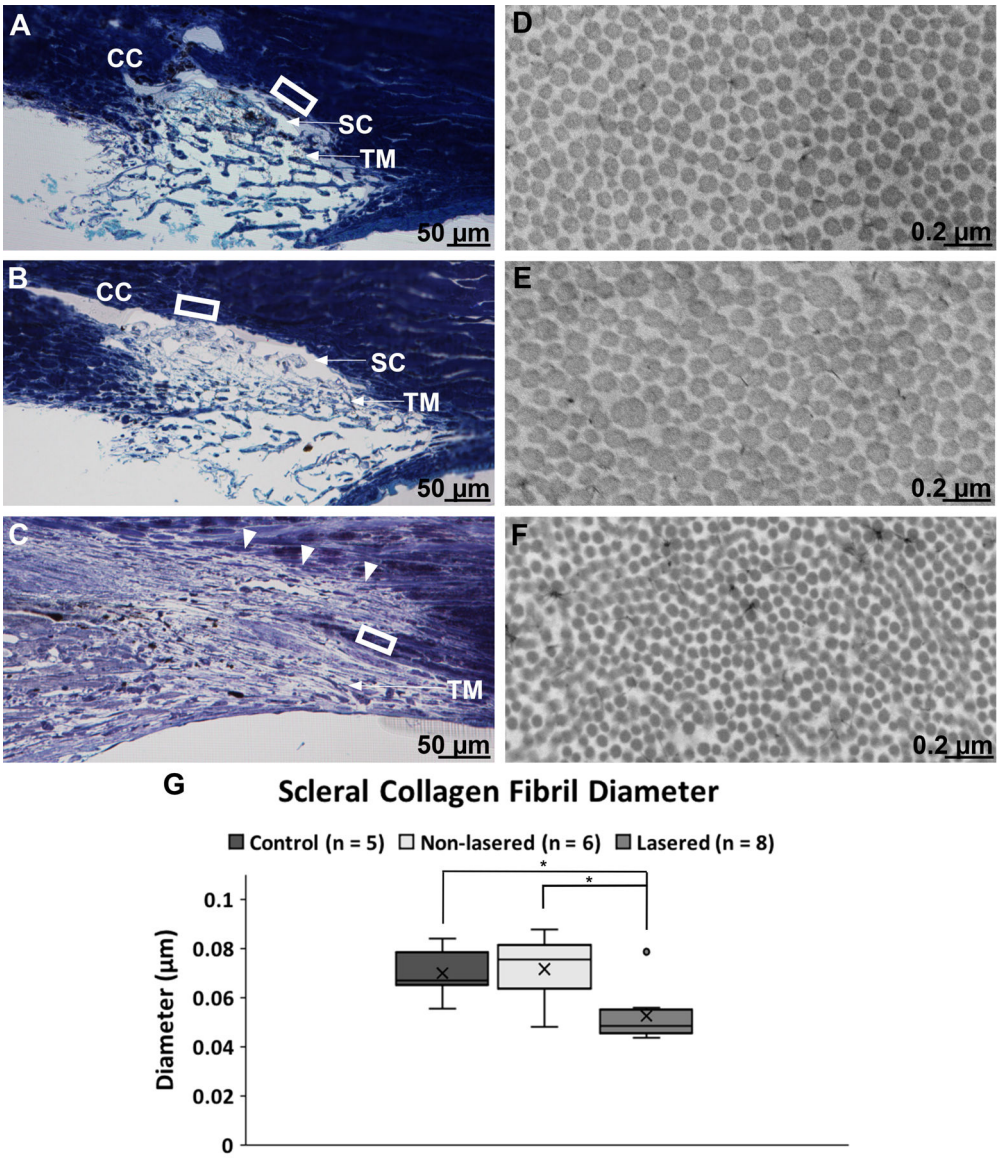

Figure 8.

Comparison of sclera between control, non-lasered, and lasered regions via light and electron microscopy. Light microscopic evaluation revealed that, compared to control (**A**) and non-lasered (**B**) regions, lasered regions (**C**) had areas of less compact organization of the scleral stroma adjacent to the trabecular meshwork (TM) (*white arrowheads*). White boxes in **A**, **B,** and **C** highlight regions of sclera adjacent to the TM where collagen fibril diameters were evaluated via electron microscopy in **D**, **E**, and **F**, respectively. CC = collector channel; SC = Schlemm's canal. **G:** A significantly smaller scleral collagen fibril diameter (49 nm, IQR: 45 – 55; $n = 8$) was observed in lasered regions when compared to control (67 nm, IQR: 65 – 78; $n = 5$; $P = 0.03$) and non-lasered regions (75 nm, IQR: 64 – 82; $n = 6$; $P = 0.02$). *Whiskers:* 1.5 interquartile range (IQR). X = mean. * $P < 0.05$.

Author Manuscript Author Manuscript Author Manuscript Author Manuscript

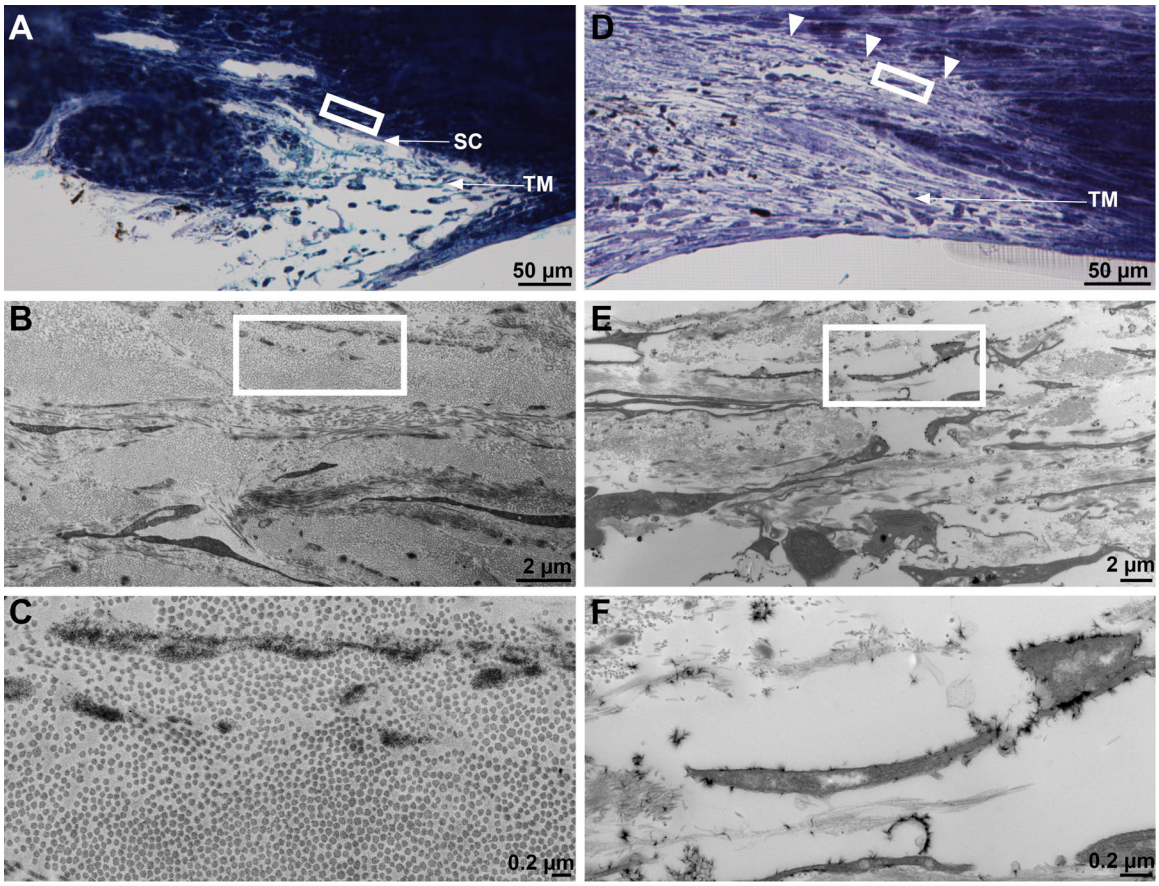

Figure 9.

Decreased collagen fibril density in the sclera of lasered eyes. **A:** A light micrograph from a representative control eye. The *white box* demarcates sclera evaluated via electron microscopy at 1000X magnification in **B**. The *white box* in **B** demarcates the region of sclera shown at higher (4000X) magnification in **C**. The sclera appears uniform, compact, and darkly staining via light microscopy (**A**), and electron microscopy reveals densely packed collagen fibrils (**B-C)**. **D:** A light micrograph from a representative lasered region of a laser-treated eye. The white box in **D** demarcates sclera evaluated via electron microcopy at 1000X magnification in **E**. The *white box* in **E** highlights a region of sclera shown at higher (4000X) magnification in **F**. Note that the sclera adjacent to the trabecular meshwork (TM), indicated by the *white arrowheads* in **D**, has more loosely organized collagen fibrils and more open spaces, compared to the sclera in control eyes. SC = Schlemm's canal.

Author Manuscript Author Manuscript Author Manuscript Author Manuscript

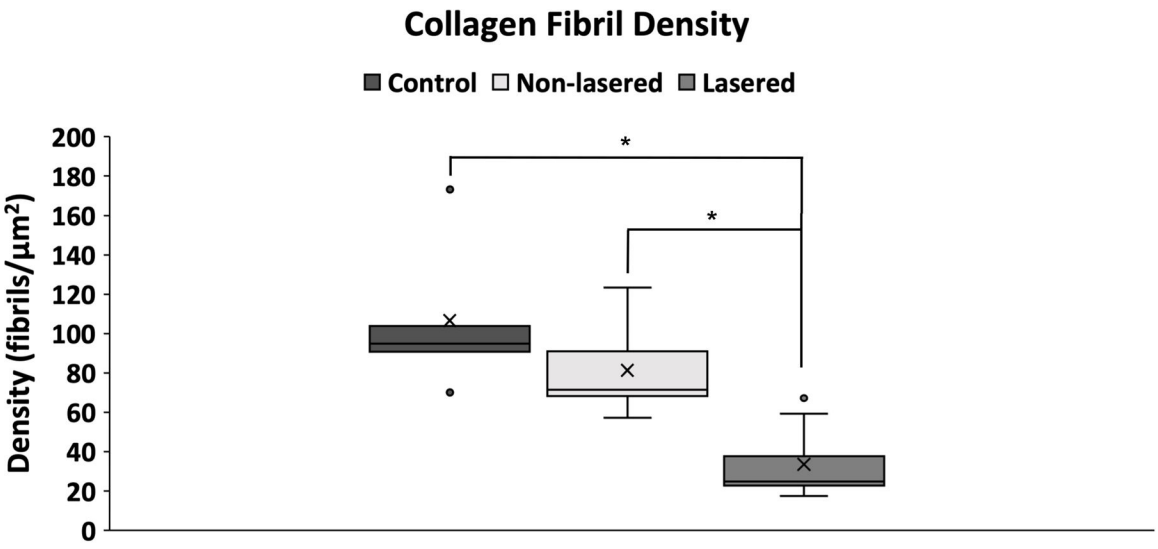

Figure 10.

Collagen fibril density decreased in lasered regions. Collagen fibril density was decreased in lasered regions of laser-treated eyes (25 fibrils/μm^2, IQR: 23 – 38; $n = 8$) compared to both control eyes (95 fibrils/μm^2, IQR: 91 – 104; $n = 5$; $P < 0.01$) and non-lasered regions of laser-treated eyes (72 fibrils/μm^2, IQR: 68 – 91; $n = 6$; $P < 0.01$; Fig. 10). *Whiskers:* 1.5 interquartile range (IQR). X = mean. * $P < 0.01$.

Author Manuscript

Author Manuscript

Author Manuscript

Author Manuscript

Table 1

IOPs and time from final laser treatment to IOP measurements in control and laser-treated monkey eyes

	Control		Laser-treated		Time from Final Laser Treatment to IOP Measurement	
Monkey	**Intermediate IOP (mmHg)**	**Final IOP (mmHg)**	**Intermediate IOP (mmHg)**	**Final IOP (mmHg)**	**Intermediate IOP (months)**	**Final IOP (months)**
1	N/A	22.0	N/A	20.0	N/A	60
2	26.5	22.0	35.8	31.0	131	147
3	23.7	29.9	30.0	31.5	130	163
4	31.5	19.6	64.8	29.8	122	164
5	22.0	27.5	28.4	31.3	131	174
6/OS			28.9	25.7	131	141
6/OD			34.5	27.5	83	93
7			34.6	19.3	134	182

Intermediate IOPs were taken after laser-treatment but 10–48 months prior to final IOPs. In comparing intermediate IOPs between laser-treated and control eyes using a Wilcoxon rank sum test, median IOPs in laser-treated eyes (34.50 mmHg, IQR: 29.45 – 35.2; $n = 7$) were significantly higher than control eyes (25.1 mmHg, IQR: 23.28 – 27.75; $n = 4$; $P = 0.04$).

Author Manuscript

Author Manuscript

Author Manuscript

Author Manuscript

Table 2

ISV number and CSA between lasered and non-lasered regions by eye

	Median ISV Number (ISVs/mm)		Median ISV CSA (μm^2)	
Eye	**Lasered**	**Non-lasered**	**Lasered**	**Non-lasered**
1	0	3.4	30	41
2	1.2	4.1	35	224
3	0	9.5	24	17
4	2.3	3.2	84	60
5	1.2	4.4	47	86
6	1.1	1.8	195	174
All Eyes	1.5	3.7	60	188

For the 6 laser-treated eyes in which measurements were conducted in both lasered and non-lasered regions, ISV number was consistently higher in non-lasered regions when comparing by eye. In comparing all lasered and non-lasered regions, lasered regions had a significantly lower number of ISVs ($P < 0.01$). CSA did not differ consistently between lasered and non-lasered regions by eye. Median ISV CSA between all lasered and non-lasered regions was not significantly different ($P > 0.05$). Median ISV number and CSA for all lasered and non-lasered regions combined is demonstrated in the final row of the table.